

Vegetation cover change as a growing driver of global leaf area index dynamics

Received: 19 July 2024

Accepted: 12 September 2025

Published online: 20 October 2025

 Check for updates

Dashan Wang ^{1,2,3}, Alan D. Ziegler ⁴, Joseph Holden ⁵,
Dominick V. Spracklen ⁶, Philippe Ciais ⁷, Liqing Peng ^{8,9} &
Zhenzhong Zeng ^{1,3} 

The ongoing four-decade increase in global leaf area index (LAI), inferred from satellite observations, suggests enhanced carbon sequestration and evaporative cooling with potential benefits that may help mitigate climate warming. However, the role of vegetation cover change in driving these trends remains debated, raising concerns about the potential effects of reforestation and deforestation on ecosystem-climate interactions. Here, we develop a data-driven framework combining satellite-based observations to quantify the contributions of vegetation cover change to LAI dynamics across space and time. We find that vegetation cover change explains $18.1 \pm 5.9\%$ of the observed LAI increase since the 1980s, with pronounced contribution from increased tree cover primarily occurring in the northern hemisphere ($33.8 \pm 3.6\%$), partially offset by deforestation mainly taking place in the southern hemisphere ($-15.7 \pm 3.1\%$). Increases are most prominent in forestation regions such as China and Europe, while the sensitivity, defined as LAI change per unit percentage of tree cover gain, is lower than declines induced by deforestation in tropical areas. Our findings reveal that vegetation cover change is already, and increasingly, shaping global LAI dynamics to a greater extent than previously recognized, with important implications for future LAI trajectory projections, model development, and climate mitigation policies.

A worldwide increase in leaf area index (LAI) has been reported based on satellite observations over the past four decades^{1–6}. This emerging signal can partially alleviate global warming by promoting vegetation productivity and enhancing the land carbon sink^{7–9}, as well as sustaining plant-driven evaporative cooling and accelerating the hydrological cycle^{10–12}. Consequently, increased LAI assumes a crucial role in climate mitigation and ecosystem resilience, drawing considerable interest in global change science¹³.

Vegetation cover change (VCC), encompassing facets including reforestation, deforestation, and cropland expansion, has the potential to directly enhance or suppress LAI increases by altering vegetation extent and function^{2,14}. While various indirect climatic and ecological factors⁴, including CO₂ fertilization^{15,16}, climate change (e.g., temperature, water availability, solar radiation)^{7,17}, nitrogen deposition¹⁸, and agricultural management practices^{4,19}, have been extensively studied as drivers of regional and global LAI increase, the specific contribution

¹State Key Laboratory of Soil Pollution Control and Safety, Southern University of Science and Technology, Shenzhen, China. ²School of Geography and Planning, Sun Yat-sen University, Guangzhou, China. ³School of Environmental Science and Engineering, Southern University of Science and Technology, Shenzhen, China. ⁴Andaman Coastal Station for Research and Development, Kasertart University, Ranong, Thailand. ⁵School of Geography, University of Leeds, Leeds, UK. ⁶School of Earth and Environment, University of Leeds, Leeds, UK. ⁷Laboratoire des Sciences du Climat et de l'Environnement, CEA/CNRS/UVSQ/Université Paris Saclay, Gif-sur-Yvette, France. ⁸Department of Geography, The University of Hong Kong, Hong Kong, China. ⁹Institute for Climate and Carbon Neutrality, The University of Hong Kong, Hong Kong, China. ✉ e-mail: zengzz@sustech.edu.cn

and impact of VCC on observed LAI changes remain contested². As the world intensifies commitment to forest restoration and conservation as nature-based solutions to combating climate change²⁰, unraveling the complexities of VCC-induced LAI increase becomes ever more critical. The urgency in doing so is underscored by reports revealing the persistent challenge of reducing deforestation despite previous efforts²¹. Enhanced understanding of the role of VCC in driving LAI changes can aid refining parameterization of vegetation processes in Earth system models, thereby improving the accuracy of projected vegetation dynamics and associated ecosystem benefits^{22,23}.

Previous modeling studies have suggested that CO₂ fertilization is the dominant contributor to the global rise in LAI^{3,15}, while the effects of VCC were estimated to account for only 4% of the observed trend³. Conversely, studies utilizing field and satellite observations have emphasized a distinct overlap between croplands and observed LAI increases, particularly prominent in China and India^{4,19}, leading to inferences that human agricultural management could potentially explain more than 33% of global LAI changes⁴. However, the influence of VCC on LAI change was blended among land management changes in their analyses. Much of the conflicting results and uncertainties may arise from the lack of comprehensive statistical exploration that can effectively separate the contributions of individual factors^{19,24}, as well as limitations in models that inadequately represent fine-scale land-use practices and parameterize physical processes^{22,25}. Specifically, large-scale forest restoration and tree planting^{26–30}, along with commodity-driven deforestation^{21,31,32}, have undoubtedly reshaped global vegetation cover¹⁴. Yet, their contribution to Earth's LAI changes remains unclear, as only a few studies have investigated the influence of VCC over limited regions^{33,34}. To date, there is a substantial lack of quantitative, data-driven attribution of LAI changes in response to VCC, raising concerns about the impact of VCC-related policies and actions for ecosystem monitoring and climate mitigation.

To tackle these challenges, we develop a framework based on statistical models that utilize satellite-observed LAI data and the vegetation continuous fields (VCF) product¹⁴ as inputs, covering the satellite era (“Methods”, Supplementary Figs. 1–5). The maximum monthly LAI³⁵ is used because the VCF data identify the vegetation composition at the local peak growing season¹⁴. First, we decompose the greenness parameters (β) within 3° × 3° grids in each year for three different land-cover categories—tree cover (β_{TC}), short vegetation (β_{SV}), and bare ground (β_{BG})—using LAI and VCF observations at the original resolution. The greenness parameters (β) represent a grid-averaged LAI value under the assumption of 100% coverage of each vegetation type within the grid cell. This is achieved using an improved Bounded-Variable Least Squares approach, which not only defines value ranges but also imposes constraints on the relative magnitudes of these three variables (Eqs. 1–3). Next, we reconstruct LAI (denoted as σ LAI) across 3° × 3° grid, regional and global scales based on the decomposed greenness parameters (β) and the proportion of each land-cover type, then calculate the trend of reconstructed LAI (δ LAI) (Eqs. 4–6).

To attribute the drivers of LAI changes more precisely, we categorize them into two distinct groups: (1) LAI change signals related exclusively to VCC (δ VC), and (2) LAI trends induced by indirect factors in areas where vegetation cover remained unchanged, calculated as the residual (δ ID = δ LAI – δ VC) (Supplementary Fig. 1). The statistical models are validated by comparing the reconstructed σ LAI and δ LAI with observations across various scales (Supplementary Figs. 6, 7 and Supplementary Table 1). In parallel, we demonstrate the robustness of our results by comparing against the annual mean LAI that is used to represent vegetation greenness, using other alternative long-term satellite products, and at variable grid spacings ranging from 0.5° × 0.5° to 5° × 5° (“Methods”). Importantly, our approach focuses on distinguishing LAI changes exclusively associated with VCC, providing solid, quantitative observational evidence of the LAI changes in

response to VCC, rather than isolating specific natural or anthropogenic factors as in previous studies.

Results and discussion

Attributing Earth's LAI changes

Globally, there has been a significant increase in satellite-observed maximum monthly LAI of 0.093 m² m⁻² decade⁻¹ (standard error of the mean (SEM) = 0.011 m² m⁻² decade⁻¹; statistical significance was assessed using a two-sided *t* test: *t*(32) = 8.12, *p* < 0.001) since the early 1980s. In agreement, our statistical model reconstructed a consistent trend of 0.094 ± 0.012 m² m⁻² decade⁻¹ (mean ± SEM; *t*(30) = 8.04, *p* < 0.001), demonstrating its robustness in capturing the temporal variation and trend of the observed LAI changes (σ LAI and δ LAI in Fig. 1a; *r* = 0.997; Relative Bias = 1.3%). At the grid-level, the reconstructed annual σ LAI shows strong correlations (*r* > 0.99) and minimal bias (< ± 0.03 m² m⁻²) in over 95% of the grids (Supplementary Fig. 6). Overall, the reconstructed δ LAI demonstrates high accuracy, particularly in areas with significant LAI changes (Supplementary Fig. 7).

The reconstructed global trend is further attributed to individual and combined drivers associated with VCC (Fig. 1b). VCC contributed 18.1 ± 5.9% of the global LAI increases (0.017 ± 0.005 m² m⁻² decade⁻¹; *t*(30) = 3.09, *p* < 0.01), with the main contribution coming from increased tree cover (25.8%), which was partially offset by reduced presence of short vegetation (–7.4%) and bare ground (–0.3%). Despite the decline in global bare ground cover¹⁴, its contribution to global LAI changes remains minimal due to its notably lower LAI parameters (β_{BG}) compared with tree cover and short vegetation (Supplementary Fig. 5). Focusing on regions where significant signals of LAI change were observed^{4,6}, such as China, Europe, India, Sahel, and Brazil, we find that δ VC can reach a mean of up to 0.030 ± 0.006 m² m⁻² decade⁻¹ (*t*(30) = 5.16, *p* < 0.001). This accounts for 20.6 ± 4.0% of the LAI change in these areas (Supplementary Fig. 8).

At the continental level, Europe stands out with the highest magnitude of areal mean δ LAI, where δ VC dominates, accounting for 54.2% (Fig. 1c, d). Asia plays the most dominant role in global LAI trends, contributing 33.0% to overall changes, with δ VC explaining 38.3% of regional variation and 12.5% of global shifts (Fig. 1d and Supplementary Table 2). VCCs in North America and Africa affect their regional LAI variations by 23.9% and 14.0%, respectively. In contrast, in South America and Oceania, the contributions of δ VC are negative (–35.9% and –20.8%, respectively), indicating a decline in LAI due to forest loss. However, this signal is outweighed by the enhanced growth of existing vegetation at scales of tens to hundreds of kilometers (Fig. 1d versus Supplementary Fig. 9). Generally, changes of tree cover fraction are the primary factor driving δ VC, except for Africa, where increases in short vegetation fraction play a more prominent role.

To ensure robustness of our findings, we tested our model under different settings (Methods). In addressing uncertainties related to the representation of vegetation greenness, we conducted additional tests using the annual mean LAI instead of the maximum monthly LAI (Supplementary Fig. 10). To assess uncertainties associated with different LAI datasets, we performed analyses using three alternative long-term satellite products (Supplementary Figs. 11–13). These tests reaffirmed the validity of the non-negligible role of δ VC in our main analysis. In addition, the effect of varying spatial analysis scales showed that the proportions of δ VC consistently fell within a similar range, reinforcing the reliability of our findings (Supplementary Table 3).

Contrasting effects of regional vegetation cover change on LAI changes

The magnitude of δ VC exhibits a noticeable latitudinal gradient, with a contrast between the two hemispheres (Fig. 1e). The overall positive δ VC globally results from LAI increases that mainly occur in the northern hemisphere (33.8 ± 3.6%; 0.031 ± 0.003 m² m⁻² decade⁻¹, *t*(30) = 9.43, *p* < 0.001), compared with LAI decreases due to forest

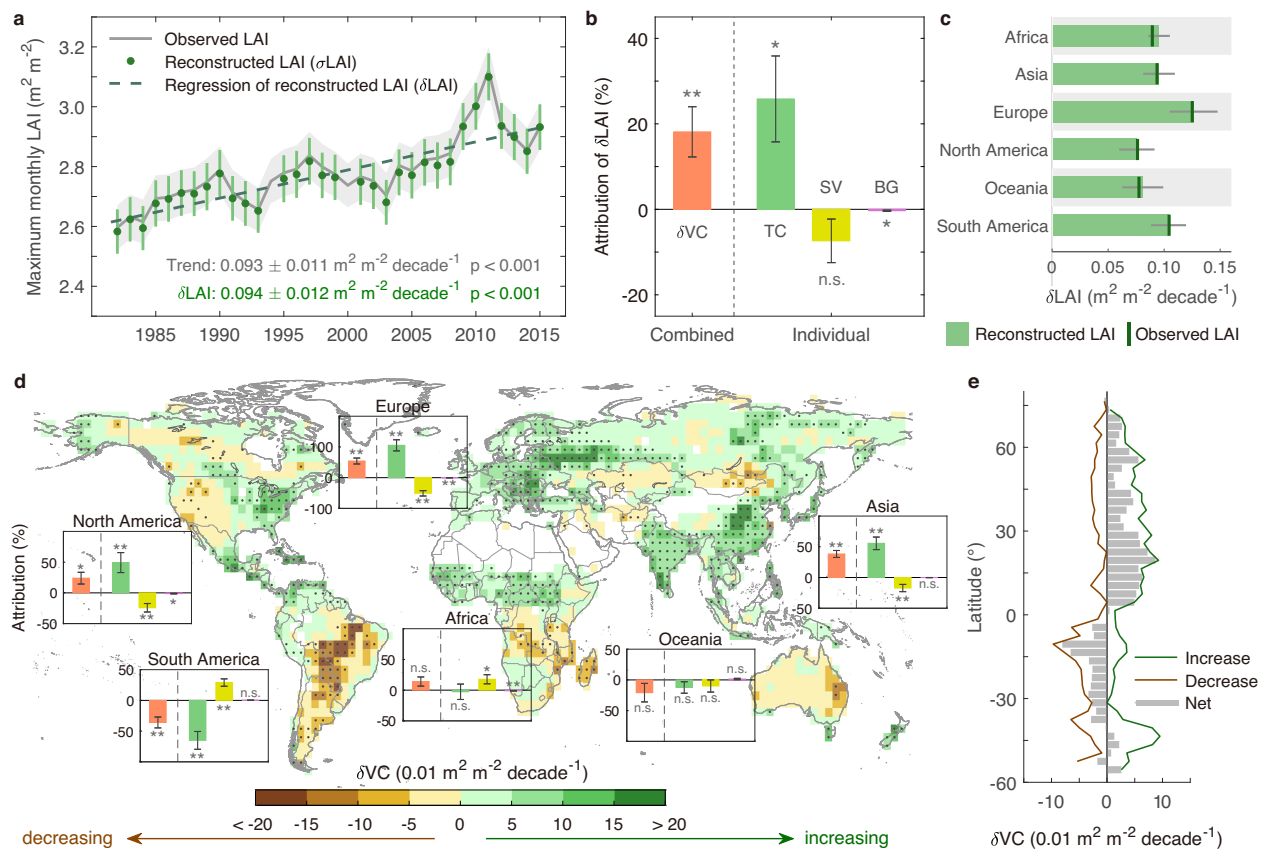


Fig. 1 | Attribution of Earth's LAI changes. **a** Temporal variation of global land average maximum monthly LAI derived from the GIMMS LAI3g data⁴⁹ (gray line, $n = 1544$ grids for each year) and the model reconstruction (σ LAI; green dots, $n = 1544$ grids) for the period 1982–2015, with gray shaded areas and green vertical bars representing the 95% confidence interval (two-sided t test) respectively. The dashed line (δ LAI) is the least squares regression of σ LAI against time (two-sided t test, $p < 0.001$). **b** Attribution of δ LAI to vegetation cover change (δ VC) and its corresponding individual drivers. Bar heights represent the mean fractional contribution of each driver, calculated as the trend in LAI change under that driver weighted by grid area, divided by the reconstructed δ LAI, and error bars indicate the standard error of the mean (SEM) of the mean contribution. Statistical significance is assessed using a two-sided t test (d.f. = 30, $n = 1544$ grids for each year),

with asterisks indicating significance levels: ** $p < 0.01$; * $p < 0.05$; n.s., not significant. **c** Magnitude (bars) and the SEM (gray horizontal lines) of the model reconstruction, as well as the mean value of observation (green vertical lines) in Africa ($n = 216$ grids), Asia ($n = 553$), Europe ($n = 174$), North America ($n = 335$), Oceania ($n = 93$), and South America ($n = 173$). **d** Spatial pattern of reconstructed δ VC at $3^\circ \times 3^\circ$ grid spacing. Dots represent statistically significant at $p < 0.01$ (two-sided t test, d.f. = 30). The insets show the attribution of δ LAI (mean \pm SEM, follows the same definition as in panel (b)) over the six continents, with sample sizes for each group match those in panel (c). **e** The latitudinal gradient of positive δ VC (increase), negative δ VC (decrease), and the net δ VC at 3° intervals. Source data are provided as a Source Data file.

loss primarily in the southern hemisphere ($-15.7 \pm 3.1\%$; $-0.014 \pm 0.003 \text{ m}^2 \text{m}^{-2} \text{decade}^{-1}$, $t(30) = -4.96$, $p < 0.001$) (Fig. 2a). The temporal variations are generally consistent with major forestation or conservation projects, including the forest recovery following land abandonment in Eastern Europe and European Russia since the late 1980s (ref. 27), the Grain for Green Program and the Natural Forest Protection Program implemented around 2000 in China^{26,29}, and the Bonn Challenge which started in 2011 (ref. 28). From 2003 to 2015, the VCC-induced LAI (σ V) reveals a substantial enhancement, consistent with the previously reported reversal of terrestrial biomass resulting from forest expansion mainly in Asia and Europe³⁶.

Spatially, clusters of positive δ VC are primarily found in recently afforested areas, spanning regions in China, Europe, the Middle Africa Climatic Transition Zone (MACTZ), Eastern Siberia, and the eastern United States, as well as in areas that experienced agricultural intensification, such as India and northern China (Fig. 1d and Supplementary Fig. 3b). The contribution of VCC could reach up to 29–73% in those areas (Fig. 2b). Notably, in China, δ VC contributes to 72.5% of the nationwide δ LAI, affirming the primary role of VCC in shaping long-term shifts in vegetation greenness of China³³. This is likely in response to national programs such as the Great Green Wall of China, which

initiated in 1978 and is expected to continue until 2050, making it the largest afforestation initiative in human history²⁹. India exhibits the highest magnitude of δ VC, due to both the positive effects of agriculture expansion and tree cover gain, along with a substantial decrease in bare ground (Fig. 2b, c). The contributions of δ VC from Russia, China, MATCZ, and the European Union to the global δ LAI exceed those of India, and these four regions collectively account for 17.1% of Earth's LAI increase (Fig. 2c and Supplementary Table 2).

In contrast, negative δ VC predominates in Brazil, Argentina, Madagascar, and the Miombo woodlands in south-central Africa (Fig. 1d). Specifically, in Brazil and Argentina, δ VC contributed to δ LAI of about -50% (Fig. 2b). Some LAI increases in these areas largely resulted from indirect factors⁴ such as CO_2 fertilization, climate change and nitrogen deposition^{3,7} (δ ID; Supplementary Fig. 9a). These indirect increases may have offset the deforestation-induced decrease in LAI at a regional scale over the past four decades (Fig. 1d versus Supplementary Fig. 9b). However, the persistence of these benefits amidst escalating disturbances cannot be guaranteed. If deforestation continues and warming intensify, the current buffering effect may weaken, leading to accelerated LAI decline and the potential disruption of tropical forest ecosystems, which are renowned for their

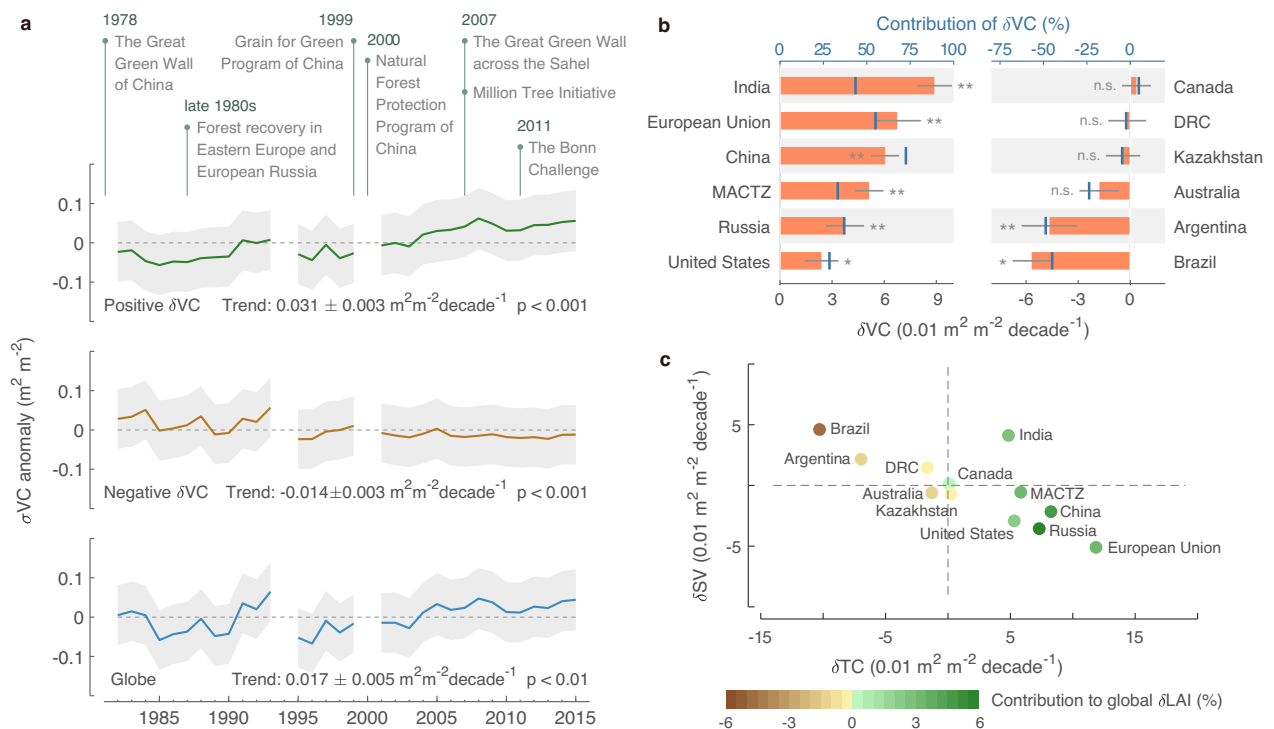


Fig. 2 | Spatial variations of vegetation cover change-induced global LAI changes. **a** Temporal anomalies of VCC-induced LAI change (σ_{VC}) are shown in grids with positive δ_{VC} , negative δ_{VC} , and globally. Gray shades represent the 95% confidence interval of σ_{VC} (two-sided t test). Trends (mean \pm SEM) of σ_{VC} and the statistical significance are assessed using a two-sided t test and presented in the figure. The names and initiate years of major VCC programs and progresses are listed (refs. 26–30). **b** Magnitude (bars) and the mean fractional contribution (vertical lines) of δ_{VC} on δ_{LAI} in main countries and regions. Bar heights represent the mean value of δ_{VC} weighted by grid area, and error bars show the SEM. The

significance of δ_{VC} is indicated by asterisks: ** $p < 0.01$; * $p < 0.05$; n.s., not significant (two-sided t test; sample numbers for each country or region are given in Supplementary Table 1). The abbreviation DRC stands for the Democratic Republic of the Congo. MACTZ, denoting the Middle Africa Climatic Transition Zone, covers a broader region comprising the Sahel and an adjacent belt of savanna climate to the south. For a comprehensive list of the countries within this zone, please refer to Supplementary Table 1. **c** Magnitude of δ_{TC} and δ_{SV} in main countries and regions, with the color denoting their contribution of δ_{VC} to global δ_{LAI} . Source data are provided as a Source Data file.

biodiversity and high productivity^{37,38}. Further assessment of the sensitivity of δ_{VC} to vegetation cover changes across continents reveals that the sensitivities to tree cover losses in South America ($-0.306 \pm 0.010 \text{ m}^2 \text{ m}^{-2} \text{ decade}^{-1}$ per 10% tree cover loss, $t(151) = 31.24$, $p < 0.001$) and Oceania (-0.360 ± 0.015 , $t(42) = 24.22$, $p < 0.001$) are notably higher than those linked with tree cover gains in Asia ($0.264 \pm 0.008 \text{ m}^2 \text{ m}^{-2} \text{ decade}^{-1}$ per 10% tree cover gain, $t(423) = 31.65$, $p < 0.001$) and Europe (0.218 ± 0.009 , $t(166) = 24.73$, $p < 0.001$) (Supplementary Fig. 14). This emphasizes the detrimental consequences of losing carbon-dense forests in tropical regions, meanwhile highlighting the urgent need for effective forest protection and management^{39,40}.

Increasing contribution of vegetation cover change over time

The contribution of VCC to LAI trends has increased progressively over time (Fig. 3a). Analyzing the time series of δ_{VC} with expanding windows since 1982, we observe a significant upward trend at a rate of $0.017 \pm 0.001 \text{ m}^2 \text{ m}^{-2} \text{ decade}^{-2}$ ($t(16) = 12.36$, $p < 0.001$) from the period 1982–1997 to 1982–2015. This increase is driven by a reduction in LAI decreases (LAI_{\downarrow}) from forest loss ($0.012 \pm 0.001 \text{ m}^2 \text{ m}^{-2} \text{ decade}^{-2}$; $t(16) = 17.23$, $p < 0.001$) and an amplification in LAI gains (LAI_{\uparrow}) from vegetation expansion ($0.005 \pm 0.001 \text{ m}^2 \text{ m}^{-2} \text{ decade}^{-2}$; $t(16) = 5.33$, $p < 0.001$). Concurrently, δ_{VC} holds an increasingly prominent role in Earth's LAI changes, following a nonlinear growth pattern over time. Globally, the fraction of total LAI changed explained by δ_{VC} increased from around ~10% before 2003 to a peak of 20.6% in 2009, followed by a slowdown in the 2010s (Fig. 3a). This fluctuation may reflect a stalling of LAI increases by indirect factors during the 2000s (ref. 24). At the

continental level, the increased magnitude and contribution of δ_{VC} from both enhanced LAI_{\uparrow} and reduced LAI_{\downarrow} are also evident in Asia, Europe, North America, and South America (Supplementary Figs. 15, 16). Meanwhile, a declining trend in vegetation gain in Africa has led to a steady weakening of δ_{VC} . Overall, our findings highlight the increasing role of VCC in driving LAI changes, particularly prominent in the 2000s.

The spatially heterogeneous trends in δ_{VC} across countries and regions reflect diverse VCC processes and geographical constraints (Supplementary Fig. 17). In areas where increases in tree cover expansion dominated VCC, such as the Loess Plateau in China, Carpathian Mountains in Europe, and eastern United States, δ_{VC} increased substantially in the 2000s, reaching 0.10 – $0.20 \text{ m}^2 \text{ m}^{-2} \text{ decade}^{-1}$. In contrasts, water-limited savannas in Central Africa exhibited a gradual long-term decline in δ_{VC} during the past four decades (Fig. 3b, c), suggesting a potential future leveling-off of vegetation greenness under increasing water constraints in newly afforested areas like the Loess Plateau^{41,42}. In northwest India, where short vegetation expansion dominates VCC, a slight decreasing trend of δ_{VC} exists (Fig. 3b, c). In regions that experienced deforestation, such as Cerrado and Gran Chaco in South America and Madagascar, the significant negative δ_{VC} exhibits a decreasing trend, reflecting a reduction in VCC-induced LAI_{\downarrow} during 1982–2015 (Fig. 3d).

Implications for nature-based solutions

The influence of VCC, which reshaped the vegetation structure worldwide over the last four decades, has significant policy

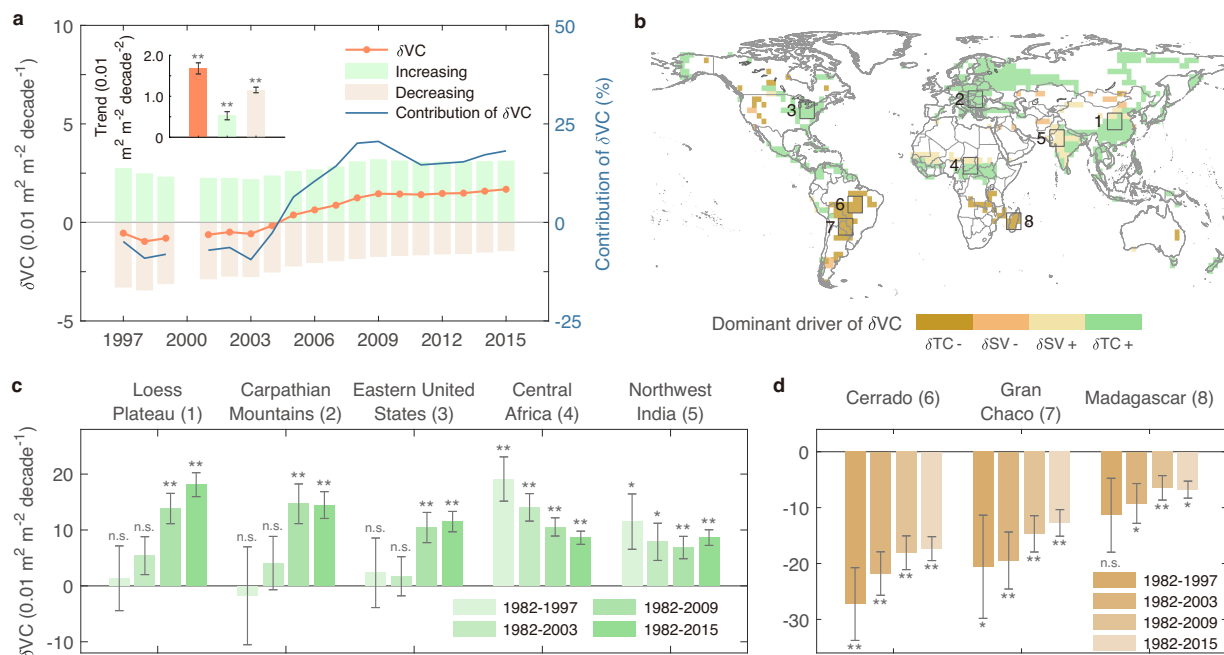


Fig. 3 | Temporal variations of vegetation cover change-induced global LAI changes. **a** Temporal dynamics of δVC (orange line), area-weighted mean δVC in grids with gross increases (LAI^+ ; green bars) and gross decreases (LAI^- ; brown bars) with expanding windows fixed starting from 1982 (left y-axis; two-sided t test, $n = 1544$ grids), as well as variations in the corresponding contributions of δVC to global LAI change (blue line; the ratio of δVC to δLAI ; right y-axis). Inset bars show trends for the accumulated δVC time series, and error bars indicate the SEM of the mean trend (two-sided t test, d.f. = 16). Trends and statistical significance were estimated using the ordinary least squares regression, with two asterisks denoting

$p < 0.001$. **b** Dominant driver of δVC in those grids with significant δVC trends. Eight typical regions with a higher magnitude of δVC are highlighted in rectangles (each covers 9 grids). **c, d** Temporal variations of δVC during four expanding windows since 1982, ending in 1997, 2003, 2009, and 2015 over the eight typical regions. Bar heights represent the area-weighted mean δVC , and error bars indicate the SEM of the mean trend. Statistical significance is assessed using a two-sided t test (d.f. = 13, 18, 24, 30, respectively), with asterisks indicating significance levels: ** $p < 0.01$; * $p < 0.05$; n.s., not significant. Source data are provided as a Source Data file.

implications^{32,39,43}. The non-negligible role of VCC-related actions in LAI increase is primarily driven by afforestation in the northern hemisphere^{26–30}. However, on a global scale, this effect is partially offset by the LAI declines associated with widespread tropical deforestation and degradation^{14,21,31}. Some regions, such as southeastern Amazonia, have transitioned from being carbon sinks to carbon sources due to forest loss and disturbance^{37,38}. Deforestation in areas like the Cerrado and Gran Chaco resulted in negative δVC values, directly countering the benefits of indirect factors and leading to a shift from LAI increase to decrease (Supplementary Figs. 2 and 9).

Apart from forest change dynamics, cropland management, such as irrigation, fertilization, and species transformation, has also affected the LAI variability without altering the vegetation cover type. A recent study⁴ highlighted that human land-use practices might contribute to more than one-third of the observed Earth's LAI increases, particularly in areas with extensive croplands, notably China (25%) and India (6.8%). Building on their conclusion that over one-third of global LAI increase is linked to direct land-use practices, our approach provides a more precise partitioning of LAI change signals. We estimate that cropland management without vegetation cover change (δSC) accounts for no more than $14.2 \pm 2.0\%$ (“Methods”; Supplementary Fig. 18a, b). This lower contribution compared to VCC is evident in China (15.6% of δSC versus 72.5% of δVC) and India (37.3% versus 43.5%), underscoring the necessity to distinguish the long-term LAI change signals induced by land-cover transition from those caused by land management alone (Supplementary Fig. 18c, d and Supplementary Table 3). Generally, agricultural intensification (management) predominated in developed regions, whereas agricultural-related LAI increase was primarily attributed to cropland expansion (VCC) in less developed regions⁴⁴.

Concerns have persisted for decades regarding how climatic drivers affect global LAI dynamics², motivated by negative feedback loops within the biosphere responding to climate change¹³. Recent findings point to a weakening or saturation trend in the observed LAI increase, along with elevated CO_2 concentration and warming in this century^{24,45}, as well as the adverse effects of extreme events and decreasing water availability on vegetation photosynthesis^{42,46}. However, relying solely on satellite-observed LAI may obscure the true effects of those drivers, as VCC can partially mask the climatic signals of LAI change at the local-to-regional scale. Our results suggest that VCC may play an increasingly important role than previously thought, implying that the impacts of indirect factors on LAI increases may be overestimated. Hence, there is an urgent need to carefully exclude VCC impacts from the broader LAI changes and revisit the underlying mechanisms governing natural vegetation dynamics. Unfortunately, the ongoing intensification of ecosystem disturbances worldwide creates uncertainty in future LAI dynamics, with potential reductions driven not only by increasingly frequent extreme events, but unchecked deforestation, agriculture expansion, urbanization, and expanding energy infrastructure^{1,21,43,47}.

Our findings contradict the commonly held belief in ecosystem models that the contribution of vegetation cover change to LAI dynamics (δVC) is minor^{1,2}. This is evident in the notable difference between the model-projected δVC of 4% (ref. 3) and our higher observational attribution of $18.1 \pm 5.9\%$. Ecosystem models likely underestimate the influence of VCC due to their omission or underrepresentation of the complex patterns of land-use practices and critical physiological processes^{2,4,22,25}, which lead to an overemphasis on the benefits of indirect factors. While VCC's influence on LAI dynamics is evident, with a majority of VCC in this study linked to direct human

activities¹⁴, our aim is not to distinguish between anthropogenic and natural changes due to the coarse resolution of observations and the complexity of their interactions. Instead, our data-driven assessment highlights the role of VCC-related nature-based solutions in shaping LAI dynamics, both historically and in future projections. These solutions—such as forest preservation, ecological restoration, and afforestation⁴⁰—support climate mitigation goals while offering co-benefits like terrestrial carbon uptake, biodiversity conservation, heat stress reduction for humans and livestock, improved ecosystem services, and greater resilience to future climate impacts^{26,39,48}.

Methods

Datasets

Vegetation cover data. The Vegetation Continuous Fields version 1 product (VCF5KYR) was adopted to provide global fine-scale fractional vegetation cover information¹⁴. This product has a $0.05^\circ \times 0.05^\circ$ spatial resolution and a yearly interval, combining the advantages of multiple satellite sensors with very high spatial resolutions. The product is available from 1982 to 2016 and features the percentage of tree cover (tall vegetation ≥ 5 m in height, abbreviated as TC), short vegetation (SV), and bare ground (BG), respectively for land pixels, with a precision of 1%, representing the vegetation composition of each pixel during the peak growing season¹⁴. The sum of the proportions of the three land-cover types for each pixel is 100%. The spatial pattern of global vegetation cover and the dominant changes in vegetation cover type are shown in Supplementary Fig. 3. Note that the years 1994 and 2000 were excluded from analyses due to a lack of VCF5KYR data (<https://lpdaac.usgs.gov/products/vcf5kyrv001/>). The broad vegetation cover classification was adopted in order to maximize the utility of the available data while ensuring the statistical significance and robustness of the results. Despite the inherent resolution limitation, our approach provides valuable information on VCC at a scale that is consistent with the LAI data.

LAI data. Our analysis involved the examination of four LAI products covering the satellite era, including the Advanced Very High-Resolution Radiometer (AVHRR) Global Inventory Monitoring and Modeling Studies (GIMMS) LAI3g dataset^{3,49}, the National Oceanic and Atmospheric Administration (NOAA) Climate Data Record (CDR)⁵⁰, the Global Land Surface Satellite (GLASS) AVHRR LAI V50 product⁵¹, and the GLOBMAP LAI V3 (ref⁵²), all of which aim to provide consistent and reliable attributions of global LAI change. Note that while LAI serves as a valuable proxy of vegetation greenness^{11,53}, it may be subject to saturation effects in areas with dense vegetation, similar to other vegetation indices^{54,55}. In addition, estimating LAI from satellite imagery comes with several well-known limitations^{2,56–59}. These include spatial resolution constraints, saturation in densely vegetated areas, orbital drift, sensor replacements, retrieval algorithm uncertainties, and disturbances from land-cover heterogeneity, cloud contamination, and background reflectance. Despite these challenges, our data-driven analysis offers critical insights into the impact of VCC on LAI, allowing us to uncover broad trends and patterns across large spatial scales.

Our findings are based on the AVHRR GIMMS LAI3g dataset^{3,49} (see Robustness Analysis), which provides a comprehensive and continuous time series of LAI during the period from 1982 to 2015. Generated based on a Feed-Forward Neural Network (FFNN) model, it has a spatial resolution of $1/12^\circ$, is a bi-monthly composite, and has global coverage. It is one of the longest series among current LAI datasets and has demonstrated good performance in representing vegetation dynamics^{3,10,11}. We first interpolated the GIMMS LAI3g into 0.05° grid spacing by using linear interpolation to fit the VCF5KYR land-cover data and averaged LAI into a monthly scale by taking the temporal mean of all valid records. We then retrieved the maximum monthly LAI that represents the peak vegetation growth³⁵ for each pixel in each

year. We calculated the annual mean LAI simultaneously to discuss the uncertainties associated with the proxy of vegetation greenness (Supplementary Fig. 10; Robustness Analysis). The quantitative attributions of long-term LAI changes were determined for the period from 1982 to 2015 to align with the availability of VCF5KYR and LAI products.

To provide a robust assessment associated with satellite-based products, we utilized LAI data from three alternative long-term satellite products to examine attributions of LAI change: NOAA CDR⁵⁰, which spans from July 1981 to the present with daily frequency and a 0.05° resolution (Supplementary Fig. 11); GLASS⁵¹, which offers 8-day LAI data with a spatial resolution of 0.05° and covers the period from 1981 to 2018 (Supplementary Fig. 12); GLOBMAP⁵², which offers biweekly LAI data during 1981–2000 and 8-day LAI data during 2001–2020 at 8 km resolution (Supplementary Fig. 13). All LAI datasets were interpolated to a 0.05° grid spacing and aggregated into monthly scales for analyses.

Disentanglement of the vegetation greenness

As shown in Supplementary Fig. 1, the main concept of our framework contains two parts. Developing such a framework is motivated by the lack of LAI observations for specific vegetation types, as existing LAI data are grid-based at a resolution of ~5 kilometers, with each grid cell representing a single value that averages across multiple vegetation types. This means the lack of information on individual vegetation types for LAI, making it difficult to quantify how sub-grid scale vegetation cover changes contribute to overall LAI variations.

The first step is elucidating the proportion of different vegetation cover types from satellite-observed LAI based on an improved Bounded-Variable Least Squares (BVLS) model⁶⁰ (Eqs. 1–3). In our study, we extended the traditional BVLS approach by not only defining value ranges for the three greenness variables (β_{TC} , β_{SV} , β_{BG}) but also imposing additional constraints on their relative magnitudes (Eq. 3 and Supplementary Fig. 19). These improvements ensured that the estimated parameters adhered to physically meaningful relationships, enhancing the stability and reliability of the results, especially under conditions of noise or multicollinearity. High-resolution satellite-observed LAI data (e.g., Supplementary Fig. 2) and the VCF5KYR product¹⁴ (Supplementary Fig. 3) during 1982–2015 are used as inputs for the statistical model. To overcome the spatial homogeneity issue raised by the coarse precision of VCF data, the percentage of TC, SV, and BG, as well as the LAI data, all at $0.05^\circ \times 0.05^\circ$ resolution, were first aggregated to $0.1^\circ \times 0.1^\circ$ cells for each year by taking the average of all valid records. These 0.1° cells were then used as input to the BVLS regression. We used $3^\circ \times 3^\circ$ grid spacing as the analysis unit and retained only the grids and their inside cells with more than 20% valid LAI and vegetation cover observations at their original resolution. For detailed discussion regarding the size of cells and grids, please refer to Robustness Analysis.

We decomposed the observed LAI to TC, SV, and BG at the $3^\circ \times 3^\circ$ grid level for each year (Supplementary Fig. 1). The following regression was established for each valid $0.1^\circ \times 0.1^\circ$ cell to account for the quantitative relationship between LAI and vegetation cover in the current $3^\circ \times 3^\circ$ grid:

$$\begin{cases} \text{LAI}_1 = \beta_{TC} \cdot \text{TC}_1 + \beta_{SV} \cdot \text{SV}_1 + \beta_{BG} \cdot \text{BG}_1 + \varepsilon_1 \\ \text{LAI}_2 = \beta_{TC} \cdot \text{TC}_2 + \beta_{SV} \cdot \text{SV}_2 + \beta_{BG} \cdot \text{BG}_2 + \varepsilon_2 \\ \dots \\ \text{LAI}_i = \beta_{TC} \cdot \text{TC}_i + \beta_{SV} \cdot \text{SV}_i + \beta_{BG} \cdot \text{BG}_i + \varepsilon_i \\ \dots \\ \text{LAI}_n = \beta_{TC} \cdot \text{TC}_n + \beta_{SV} \cdot \text{SV}_n + \beta_{BG} \cdot \text{BG}_n + \varepsilon_n \end{cases} \quad (1)$$

where n is the number of valid cells with a maximum of 900; LAI_i is the satellite-observed LAI value at cell i ; TC_i , SV_i , and BG_i are the percentage of TC, SV, and BG at cell i , respectively, and their sum

equals 100%; β_{TC} , β_{SV} , and β_{BG} represent the estimated LAI parameter (in $m^2 m^{-2}$) of the current $3^\circ \times 3^\circ$ grid for assumed 100% coverage of TC, SV, and BG, respectively. Our improved BVLS model solves the linear least-squares regression with upper and lower bounds on the parameters (i.e., β_{TC} , β_{SV} , and β_{BG}), given as:

$$\min_{1 \leq x \leq u} \|Ax - b\|_2 \quad (2)$$

where A is an n-by-3 matrix of observed vegetation cover, b is an n-by-1 vector of observed LAI. Specifically, the parameters are constrained by the following inequality with upper and lower (non-negative) limits:

$$0 < \beta_{BG} \leq \beta_{SV} \leq \beta_{TC} \leq \beta_{max} \quad (3)$$

β_{max} was defined individually for each grid in each year based on the observation. This inequality was verified using a stratified random-sample approach (details refer to Supplementary Fig. 19). The significance of F-statistics (*p*-value) and the coefficient of determination (R^2) for the BVLS model were calculated to show the goodness of fit in estimating vegetation greenness parameters. The F-test, with a significance level of *p*-value < 0.05, is implemented to determine whether the model disentangles the LAI parameters better than random chance. While the R^2 reflects how well the model explains the pixel-level (0.1°) LAI variation using the grid-level averaged greenness parameters (β) within a $3^\circ \times 3^\circ$ grid. Note that the R^2 value could be negative, indicating that the improved BVLS model with constraints is not appropriate for the samples.

The improved BVLS model was established and solved in each $3^\circ \times 3^\circ$ grid for each year. The models with low confidence were removed based on the model parameters (i.e., a *p*-value of F-statistics > 0.05 and/or negative R^2). Grids were retained only if they had at least 16 years of credible BVLS models during the study period. Overall, there are 1544 valid grids left after the model quality assessment, accounting for 96.0% of all grids. Among them, 1299 grids (80.8%) have valid results in all 32 years (the years 1994 and 2000 were excluded from analyses due to a lack of VCF data). The model performs better (i.e., exhibits higher R^2 values) in regions with LAI increase hotspots and/or significant vegetation cover change (e.g., East Asia, South Asia, Europe, Sahel, eastern South America, eastern Australia), while it shows lower R^2 in areas with dense, uniform vegetation (e.g., the Amazon and Congo forests, and high-latitude tundra), likely due to limited variability in vegetation composition (Supplementary Fig. 4). The invalid grids are mainly located in coastal areas and tropical rainforests (Supplementary Fig. 4). Based on the improved BVLS statistical model and the high-resolution satellite-observed LAI and VCF data, we successfully disentangled the β_{TC} , β_{SV} , and β_{BG} parameters for each $3^\circ \times 3^\circ$ grid and each year (Supplementary Fig. 5).

Attribution of Earth’s LAI response to vegetation cover change

In the second step of our framework, we reconstructed annual LAI values by using the parameters retrieved from the BVLS model. For each $3^\circ \times 3^\circ$ grid in each year, the LAI value (σLAI ; in $m^2 m^{-2}$) was calculated as:

$$\sigma\text{LAI} = \beta_{TC} \cdot \text{TC} + \beta_{SV} \cdot \text{SV} + \beta_{BG} \cdot \text{BG} \quad (4)$$

where TC, SV, and BG are the mean proportion (%) of tree cover, short vegetation, and bare ground averaged from the valid cells in the current grid. For regional and global analyses, the grid-level estimations of LAI were aggregated by taking the area-weighted average approach, with the upper and lower ranges of the 95% confidence interval being estimated. The long-term trends of reconstructed LAI (refer to as δLAI) were derived by using linear regression during the study period at the grid, regional and global scales. The upper and lower ranges of δLAI were estimated based on the standard error of the mean. Generally, the

reconstructed δLAI performs very well in reproducing the trend and variation of the observed LAI dynamics across the global, continental, and regional scales (details refer to Validation).

To attribute the reconstructed LAI trends to drivers related to VCC, we differentiated Eq. (4) with respect to the year (denoted as *y*), as follows:

$$\begin{aligned} \delta\text{LAI} = \frac{\partial\sigma\text{LAI}}{\partial y} &= \frac{\partial\beta_{TC}}{\partial y} \cdot \overline{\text{TC}} + \frac{\partial\text{TC}}{\partial y} \cdot \overline{\beta_{TC}} + \frac{\partial\beta_{SV}}{\partial y} \cdot \overline{\text{SV}} \\ &+ \frac{\partial\text{SV}}{\partial y} \cdot \overline{\beta_{SV}} + \frac{\partial\beta_{BG}}{\partial y} \cdot \overline{\text{BG}} + \frac{\partial\text{BG}}{\partial y} \cdot \overline{\beta_{BG}} \end{aligned} \quad (5)$$

where the overbar denotes the multi-year average value of the variable. On the right-hand side of Eq. (5), the six terms represent the changes in reconstructed LAI associated with the changes in the greenness of tree cover (β_{TC}), the proportion of tree cover (TC), the greenness of short vegetation (β_{SV}), the proportion of short vegetation (SV), the greenness of bare ground (β_{BG}) and the proportion of bare ground (BG), respectively.

The reconstructed δLAI was further attributed to vegetation cover change (δVC), given by:

$$\delta\text{VC} = \frac{\partial\text{TC}}{\partial y} \cdot \overline{\beta_{TC}} + \frac{\partial\text{SV}}{\partial y} \cdot \overline{\beta_{SV}} + \frac{\partial\text{BG}}{\partial y} \cdot \overline{\beta_{BG}} \quad (6)$$

and the contributions of VCC were calculated as the ratio of δVC to δLAI . Similarly, the attributions of the changes in the proportion of tree cover ($\frac{\partial\text{TC}}{\partial y} \cdot \overline{\beta_{TC}}$), short vegetation ($\frac{\partial\text{SV}}{\partial y} \cdot \overline{\beta_{SV}}$) and bare ground ($\frac{\partial\text{BG}}{\partial y} \cdot \overline{\beta_{BG}}$) were calculated at regional and global scales. The remaining part (δID) represents the LAI changes in constant vegetation, which is largely influenced by indirect factors, as given by:

$$\delta\text{ID} = \frac{\partial\beta_{TC}}{\partial y} \cdot \overline{\text{TC}} + \frac{\partial\beta_{SV}}{\partial y} \cdot \overline{\text{SV}} + \frac{\partial\beta_{BG}}{\partial y} \cdot \overline{\text{BG}} \quad (7)$$

The interannual variations of the VCC-induced LAI (σVC_y ; in $m^2 m^{-2}$) could be reconstructed using a variable-controlling approach⁶¹ by fixing the greenness of tree cover, short vegetation and bare ground as multi-year average values:

$$\sigma\text{VC}_y = \overline{\beta_{TC}} \cdot \text{TC}_y + \overline{\beta_{SV}} \cdot \text{SV}_y + \overline{\beta_{BG}} \cdot \text{BG}_y \quad (8)$$

The anomalies of σVC during the study period (e.g., Fig. 3a) were then obtained by subtracting the multi-year mean from the resulting time series. The variable-controlling approach was also applied spatially to calculate the contribution of LAI change within specific continents, countries, or regions to global δLAI (Fig. 2c and Supplementary Table 2).

Estimating potential effect of stable cropland and managed forest

The global map of cropland extent⁶² spanning from 2003 to 2019, with a spatial resolution of 0.00025° , was utilized to delineate the extent of stable cropland without VCC signals. The original data were aggregated into 3° grid spacing using the area-weighted average approach, generating a global map showing the proportion of stable cropland (Supplementary Fig. 18a). Assuming that the LAI change of these areas is solely driven by human land-use practices, we estimated the potential contribution of cropland management ($\delta\text{SC} = \frac{\partial\beta_{SV}}{\partial y} \cdot \text{SC}$) globally and regionally, where SC represents the proportion of stable cropland at the grid level. Note that this assumption may lead to an overestimation of the contribution by disregarding the background LAI change from indirect factors like CO_2 fertilization, climate change and nitrogen deposition.

Validation

Our statistical models were validated for their ability to reproduce the characteristics of α LAI and δ LAI through comparisons with satellite-derived observations. At the grid level, the reconstructed annual α LAI shows high correlation coefficients ($r > 0.99$ for over 95.5% of valid $3^\circ \times 3^\circ$ grids; Supplementary Fig. 6a) and minimal bias ($< \pm 0.03 \text{ m}^2 \text{ m}^{-2}$ for over 95.3% of grids; Supplementary Fig. 6b). Only slight overestimations occur in semi-arid regions, such as Central Asia and Sahel, while minor underestimations are mainly observed in tropical areas. For the reconstructed δ LAI, more than 90% of the grids exhibit a bias of less than $\pm 0.01 \text{ m}^2 \text{ m}^{-2} \text{ decade}^{-1}$, with particularly low bias in grids with significant LAI changes (Supplementary Fig. 7). These results indicate that while the pixel-level fit of BVLS model may be moderate (R^2 value of ~ 0.5 in Supplementary Fig. 4), our framework still captures grid-level signals effectively in terms of magnitude and interannual variability, as evidenced by high correlation coefficients and low bias metrics. Note that our attribution analysis focus on LAI dynamics at the $3^\circ \times 3^\circ$ grid-level, and applying the estimated grid-average β values to disentangle and attribute LAI at finer scales (e.g., $0.1^\circ \times 0.1^\circ$ pixels) may introduce uncertainty.

Overall, the results show high-quality performance globally with a high correlation coefficient ($r = 0.997$, $p < 0.001$) and low relative bias (1.3%) (Fig. 1a and Supplementary Table 1) between the reconstructed annual LAI and the observations. On a continental scale, our reconstruction is robust in capturing the temporal variation and trend of the observed LAI, with correlation coefficient values varying from 0.977 to 0.999; and relative bias ranged between -0.9% and 6.7% (Fig. 1c and Supplementary Table 1). In evaluating the model performance of the largest countries and regions, we show that our model had strong capability across most countries/regions, with correlation coefficient values larger than 0.97 and relative biases of less than 6% (Supplementary Table 1). The model is relatively weak in reproducing the trend of observed LAI change in Argentina and the Democratic Republic of the Congo. This difficulty likely stems from the low coefficient of determination for the BVLS model that was induced by the spatial homogeneity of vegetation cover in those grids.

The robustness analyses further confirmed the quality of our statistical models by demonstrating similar results when using the annual mean LAI ($r = 0.990$, $p < 0.001$; Supplementary Fig. 10), the NOAA CDR LAI product ($r = 0.993$, $p < 0.001$; Supplementary Fig. 11), the GLASS LAI product ($r = 0.968$, $p < 0.001$; Supplementary Fig. 12), and the GLOBMAP LAI product ($r = 0.990$, $p < 0.001$; Supplementary Fig. 13). For the three alternative LAI products, the reconstructed δ LAI also exhibits a low bias of less than $\pm 0.01 \text{ m}^2 \text{ m}^{-2} \text{ decade}^{-1}$ in 94.9%, 94.4%, and 81.6% of the grids, with particularly low bias in grids exhibiting significant LAI changes (Supplementary Fig. 20).

Robustness analysis

Grid spacing. Initially, we conducted our analysis using a grid spacing of $0.5^\circ \times 0.5^\circ$ as the analysis unit, with each grid containing up to 100 samples at the original $0.05^\circ \times 0.05^\circ$ resolution. However, during the application of the improved BVLS models to those samples, we encountered approximately 40% of grids that produced models with low confidence, as indicated by a p -value of F -statistics > 0.05 and/or negative R^2 (Supplementary Table 3). This can be attributed to the homogeneity of vegetation cover fraction caused by the relatively low precision (1%) of the VCF product¹⁴. At a local scale (i.e., $0.5^\circ \times 0.5^\circ$ grid), many $0.05^\circ \times 0.05^\circ$ cells shared the same fraction of tree cover and/or short vegetation due to the landscape similarities, yet exhibited different satellite-observed LAI values.

To tackle the issue of spatial homogeneity, we implemented a strategy involving spatial averaging of vegetation cover fractions and an increase in the number of samples at the grid level. We conducted experiments with various settings for grids and cells (Supplementary Table 3). Initially, the percentages of TC, SV, and BG, along with the LAI

values at $0.05^\circ \times 0.05^\circ$ resolution, were aggregated to cells ranging from $0.1^\circ \times 0.1^\circ$ to $0.5^\circ \times 0.5^\circ$ for each year. This involved calculating the average of all valid records within each cell. Subsequently, the BVLS models were established and solved at the grid level, with grid size ranging from $1^\circ \times 1^\circ$ to $5^\circ \times 5^\circ$. Across different combinations of grid and cell sizes, the reconstructed contributions of δ VVC consistently ranged from 18.0% to 23.5%, underscoring the non-negligible role of VCC in global LAI increasing (Supplementary Table 3). Importantly, the robustness of our findings was not affected by the choice of analysis unit or spatial average window. Finally, we present the results based on a $3^\circ \times 3^\circ$ grid spacing with a $0.1^\circ \times 0.1^\circ$ spatial average window, which yielded the highest ratio of valid grids (96.0%) and a low bias (1.3%) in the reconstruction of δ LAI.

Maximum monthly LAI and annual mean LAI. To assess the robustness of our proxy indicator of vegetation greenness, we investigated the uncertainties associated with different indices, comparing the results derived from annual mean LAI to those from maximum monthly LAI (Supplementary Fig. 8). The reconstructed global trend in annual mean LAI ($0.030 \pm 0.007 \text{ m}^2 \text{ m}^{-2} \text{ decade}^{-1}$; $t(30) = 4.18$, $p < 0.001$) agrees well with the observation; and 97.3% of all grids are retained after the quality control. Of the observed global LAI increase, $29.7\% \pm 12.7\%$ ($t(30) = 2.37$, $p = 0.02$) can be attributed to δ VVC, confirming the substantial impact of VCC. Furthermore, the spatial distribution of δ VVC demonstrates a high level of consistency (Fig. 1d versus Supplementary Fig. 8b). We report the results based on the maximum monthly LAI due to the following considerations: (1) it represents the peak vegetation greenness during the local peak growing season, a period identified by the vegetation fields data¹⁴; (2) it can better capture the interannual changes in the greenness of croplands and plantations with different cropping cycles, making it suitable for a global study³⁵; (3) it is less affected by missing data and can be easily retrieved without subjectively defining a growing season or dealing with multiple growing seasons; and (4) the results have higher statistical significances compared with those derived from annual mean LAI.

LAI products. We performed the analysis using NOAA CDR⁵⁰, GLASS⁵¹ and GLOBMAP⁵² as alternative products to the GIMMS LAI3g⁴⁹ to test the uncertainties associated with different satellite-based datasets. Similarly, the reconstructed δ LAI based on these three datasets captures the observed magnitude and temporal variation of global vegetation greenness satisfactorily (Supplementary Figs. 11–13). Our findings consistently indicate that δ VVC accounts for $14.6 \pm 5.5\%$ ($t(30) = 2.88$, $p = 0.007$), $34.5 \pm 10.4\%$ ($t(30) = 3.30$, $p = 0.003$) and $28.6 \pm 11.8\%$ ($t(30) = 2.44$, $p = 0.021$) of δ LAI based on the NOAA CDR, the GLASS and the GLOBMAP products, respectively, reaffirming the validity of the importance of δ VVC in our main analysis. However, we observed an abrupt shift of LAI value around the year 2000 for these products (Supplementary Figs. 11c, 12c, 13c). The shift might be caused by limitations associated with sensor degradation and retrieval processes^{2,56–59,63}. Given the potential impact of this issue on the estimation of long-term LAI change during 1982–2015 (e.g., the widespread LAI increasing signals across the globe in Supplementary Fig. 11a), we reported the assessment derived from the GIMMS LAI3g product while using the results from the NOAA CDR, GLASS, and GLOBMAP products as robustness tests.

Reporting summary

Further information on research design is available in the Nature Portfolio Reporting Summary linked to this article.

Data availability

The VCF5KYR product is publicly available at <https://lpdaac.usgs.gov/products/vcf5kyrv001/>. The four LAI products (GIMMS LAI3g, NOAA

CDR, GLASS, GLOMAP) are available at <https://sites.bu.edu/cliveg/datacodes/>, <https://www.ncei.noaa.gov/products/climate-data-records/leaf-area-index-and-fapar>, <http://www.glass.umd.edu/>, and <https://zenodo.org/records/4700264>, respectively. The global cropland maps are publicly available from <https://glad.umd.edu/dataset/croplands>. Source data are provided in this paper.

Code availability

The custom MATLAB (R2023a) scripts written to analyze the data and generate figures are available at figshare⁶⁴ (<https://doi.org/10.6084/m9.figshare.24050241>).

References

- IPCC Climate Change 2022: Mitigation of climate change. *Contribution of Working Group III to the Six Assessment Report of the Intergovernmental Panel on Climate Change*, (eds Shukla, P. R., et al.) (Cambridge Univ. Press, 2022).
- Piao, S. et al. Characteristics, drivers and feedbacks of global greening. *Nat. Rev. Earth Environ.* **1**, 14–27 (2020).
- Zhu, Z. et al. Greening of the Earth and its drivers. *Nat. Clim. Change* **6**, 791–795 (2016).
- Chen, C. et al. China and India lead in greening of the world through land-use management. *Nat. Sustain.* **2**, 122–129 (2019).
- Myneni, R. B., Keeling, C. D., Tucker, C. J., Asrar, G. & Nemani, R. R. Increased plant growth in the northern high latitudes from 1981 to 1991. *Nature* **386**, 698–702 (1997).
- Cortés, J. et al. Where are global vegetation greening and browning trends significant?. *Geophys. Res. Lett.* **48**, e2020GL091496 (2021).
- Nemani, R. R. et al. Climate-driven increases in global terrestrial net primary production from 1982 to 1999. *Science* **300**, 1560–1563 (2003).
- Piao, S. et al. Lower land-use emissions responsible for increased net land carbon sink during the slow warming period. *Nat. Geosci.* **11**, 739–743 (2018).
- Chen, J. M. et al. Vegetation structural change since 1981 significantly enhanced the terrestrial carbon sink. *Nat. Commun.* **10**, 4259 (2019).
- Zeng, Z. et al. Climate mitigation from vegetation biophysical feedbacks during the past three decades. *Nat. Clim. Change* **7**, 432–436 (2017).
- Zeng, Z. et al. Impact of Earth greening on the terrestrial water cycle. *J. Clim.* **31**, 2633–2650 (2018).
- Alkama, R. et al. Vegetation-based climate mitigation in a warmer and greener World. *Nat. Commun.* **13**, 606 (2022).
- Steffen, W. et al. The emergence and evolution of Earth System Science. *Nat. Rev. Earth Environ.* **1**, 54–63 (2020).
- Song, X.-P. et al. Global land change from 1982 to 2016. *Nature* **560**, 639–643 (2018).
- Mao, J. et al. Human-induced greening of the northern extratropical land surface. *Nat. Clim. Change* **6**, 959–963 (2016).
- Walker, A. P. et al. Integrating the evidence for a terrestrial carbon sink caused by increasing atmospheric CO₂. *N. Phytol.* **229**, 2413–2445 (2021).
- Yuan, W. et al. Increased atmospheric vapor pressure deficit reduces global vegetation growth. *Sci. Adv.* **5**, eaax1396 (2019).
- Wang, R. et al. Global forest carbon uptake due to nitrogen and phosphorus deposition from 1850 to 2100. *Glob. Change Biol.* **23**, 4854–4872 (2017).
- Chen, T. et al. Land management explains the contrasting greening pattern across China-Russia border based on Paired Land Use Experiment approach. *J. Geophys. Res. Biogeosci.* **127**, e2021JG006659 (2022).
- UN Climate Change Conference, Glasgow leaders' declaration on forests and land use. <https://ukcop26.org/glasgow-leaders-declaration-on-forests-andland-use/> (2021).
- Feng, Y. et al. Doubling of annual forest carbon loss over the tropics during the early twenty-first century. *Nat. Sustain.* **5**, 444–451 (2022).
- Bonan, G. B. & Doney, S. C. Climate, ecosystems, and planetary futures: The challenge to predict life in Earth system models. *Science* **359**, eaam8328 (2018).
- Wang, D. & Zeng, Z. Urgent need to improve modelled sensitivity of evaporation to vegetation change. *Nat. Water* **2**, 211–214 (2024).
- Wang, S. et al. Recent global decline of CO₂ fertilization effects on vegetation photosynthesis. *Science* **370**, 1295–1300 (2020).
- Jiang, M., Caldararu, S., Zaehle, S., Ellsworth, D. S. & Medlyn, B. E. Towards a more physiological representation of vegetation phosphorus processes in land surface models. *N. Phytol.* **222**, 1223–1229 (2019).
- Liu, J., Li, S., Ouyang, Z., Tam, C. & Chen, X. Ecological and socio-economic effects of China's policies for ecosystem services. *Proc. Natl. Acad. Sci. USA* **105**, 9477–9482 (2008).
- Potapov, P. V. et al. Eastern Europe's forest cover dynamics from 1985 to 2012 quantified from the full Landsat archive. *Remote Sens. Environ.* **159**, 28–43 (2015).
- Verdone, M. & Seidl, A. Time, space, place, and the Bonn Challenge global forest restoration target. *Restor. Ecol.* **25**, 903–911 (2017).
- Lu, F. et al. Effects of national ecological restoration projects on carbon sequestration in China from 2001 to 2010. *Proc. Natl. Acad. Sci. USA* **115**, 4039–4044 (2018).
- Goffer, D., Sinare, H. & Gordon, L. J. The Great Green Wall for the Sahara and the Sahel Initiative as an opportunity to enhance resilience in Sahelian landscapes and livelihoods. *Reg. Environ. Change* **19**, 1417–1428 (2019).
- Zhou, L. et al. Widespread decline of Congo rainforest greenness in the past decade. *Nature* **509**, 86–90 (2014).
- Lewis, S. L., Edwards, D. P. & Galbraith, D. Increasing human dominance of tropical forests. *Science* **349**, 827–832 (2015).
- Hua, W. et al. Observational quantification of climatic and human influences on vegetation greening in China. *Remote Sens.* **9**, 425 (2017).
- Wang, J. A. & Friedl, M. A. The role of land cover change in Arctic-Boreal greening and browning trends. *Environ. Res. Lett.* **14**, 125007 (2019).
- Huang, K. et al. Enhanced peak growth of global vegetation and its key mechanisms. *Nat. Ecol. Evol.* **2**, 1897–1905 (2018).
- Liu, Y. Y. et al. Recent reversal in loss of global terrestrial biomass. *Nat. Clim. Change* **5**, 470–474 (2015).
- Hubau, W. et al. Asynchronous carbon sink saturation in African and Amazonian tropical forests. *Nature* **579**, 80–87 (2020).
- Gatti, L. V. et al. Amazonia as a carbon source linked to deforestation and climate change. *Nature* **595**, 388–393 (2021).
- IPCC *Special Report on Climate Change and Land*. (eds Shukla, P. R. et al.) (IPCC, 2019).
- Cook-Patton, S. C. et al. Protect, manage and then restore lands for climate mitigation. *Nat. Clim. Chang.* **11**, 1027–1034 (2021).
- Feng, X. et al. Revegetation in China's Loess Plateau is approaching sustainable water resource limits. *Nat. Clim. Chang.* **6**, 1019–1022 (2016).
- Feng, X. et al. Recent leveling off of vegetation greenness and primary production reveals the increasing soil water limitations on the greening Earth. *Sci. Bull.* **66**, 1462–1472 (2021).
- McDowell, N. G. et al. Pervasive shifts in forest dynamics in a changing world. *Science* **368**, eaaz9463 (2020).
- Gao, X., Liang, S. & He, B. Detected global agricultural greening from satellite data. *Agric. Meteorol.* **276**, 107652 (2019).
- Huang, M. et al. Air temperature optima of vegetation productivity across global biomes. *Nat. Ecol. Evol.* **3**, 772–779 (2019).
- Li, X. et al. Vegetation greenness in 2023. *Nat. Rev. Earth Environ.* **5**, 241–243 (2024).

47. Wei, S., Chen, Y. & Zeng, Z. An unexpectedly large proportion of photovoltaic facilities installed on cropland. *Innov. Energy* **2**, 100070 (2025).
 48. Griscom, B. W. et al. Natural climate solutions. *Proc. Natl. Acad. Sci. USA* **114**, 11645–11650 (2017).
 49. Zhu, Z. et al. Global data sets of vegetation leaf area index (LAI)3g and fraction of photosynthetically active radiation (FPAR)3g derived from global inventory modeling and mapping studies (GIMMS) normalized difference vegetation index (NDVI3g) for the period 1981 to 2011. *Remote Sens.* **5**, 927–948 (2013).
 50. Claverie, M., Matthews, J., Vermote, E. & Justice, C. A 30+ year AVHRR LAI and FAPAR climate data record: Algorithm description and validation. *Remote Sens.* **8**, 263 (2016).
 51. Liang, S. et al. The Global Land Surface Satellite (GLASS) product suite. *Bull. Am. Meteorol. Soc.* **102**, E323–E337 (2021).
 52. Liu, Y., Liu, R. & Chen, J. M. Retrospective retrieval of long-term consistent global leaf area index (1981–2011) from combined AVHRR and MODIS data. *J. Geophys. Res. Biogeosci.* **117**, G04003 (2012).
 53. Forzieri, G., Alkama, R., Miralles, D. G. & Cescatti, A. Satellites reveal contrasting responses of regional climate to the widespread greening of Earth. *Science* **356**, 1180–1184 (2017).
 54. Forkel, M. et al. Trend change detection in NDVI time series: effects of inter-annual variability and methodology. *Remote Sens.* **5**, 2113–2144 (2013).
 55. Smith, W. K., Fox, A. M., MacBean, N., Moore, D. J. P. & Parazoo, N. C. Constraining estimates of terrestrial carbon uptake: new opportunities using long-term satellite observations and data assimilation. *N. Phytol.* **225**, 105–112 (2020).
 56. de Jong, R., Verbesselt, J., Schaepman, M. E. & De Bruin, S. Trend changes in global greening and browning: contribution of short-term trends to longer-term change. *Glob. Change Biol.* **18**, 642–655 (2012).
 57. Jiang, C. et al. Inconsistencies of interannual variability and trends in long-term satellite leaf area index products. *Glob. Change Biol.* **23**, 4133–4146 (2017).
 58. Fang, H., Baret, F., Plummer, S. & Schaepman-Strub, G. An overview of global leaf area index (LAI): Methods, products, validation, and applications. *Rev. Geophys.* **57**, 739–799 (2019).
 59. Jeong, S. et al. Persistent global greening over the last four decades using novel long-term vegetation index data with enhanced temporal consistency. *Remote. Sens. Environ.* **311**, 114282 (2024).
 60. Stark, P. B. & Parker, R. L. Bounded-variable least-squares: an algorithm and applications. *Comput. Stat.* **10**, 129–129 (1995).
 61. Jin, Y. et al. Decreasing relative humidity dominates a reversal of decreasing pan evaporation in mainland China after 1989. *J. Hydrol.* **608**, 127641 (2022).
 62. Potapov, P. et al. Global maps of cropland extent and change show accelerated cropland expansion in the twenty-first century. *Nat. Food* **3**, 19–28 (2022).
 63. Tian, F. et al. Evaluating temporal consistency of long-term global NDVI datasets for trend analysis. *Remote. Sens. Environ.* **163**, 326–340 (2015).
 64. Wang, D. Vegetation cover change as a growing driver of global leaf area index dynamics. [figshare <https://doi.org/10.6084/m9.figshare.24050241>](https://doi.org/10.6084/m9.figshare.24050241) (2025).
- Technology Project for Sustainable Development in Special Innovation (KCXFZ20230731093403008), Guangdong Basic and Applied Basic Research Foundation (2022A1515240070), the Shenzhen Key Laboratory of Precision Measurement and Early Warning Technology for Urban Environmental Health Risks (ZDSYS20220606100604008), the high-level special funds provided by Southern University of Science and Technology (G03034K001; G030290001), and the funding agencies of Zhejiang Province and Ningbo Municipality through the program "Novel Technologies for Joint Pollution Reduction and Carbon Sequestration". Z.Z. thanks Otto Poon Research Institute for Climate-Resilient Infrastructure at the Hong Kong Polytechnic University for providing the visiting fellowship. This work is supported with the High Performance Computing Centers at SUSTech.

Author contributions

Z.Z. and D.W. designed the research; D.W. performed the analysis and wrote the draft. Z.Z. and A.D.Z. provided key input for the article structure. J.H., D.V.S., P.C. and L.P. contributed to the interpretation of the results and the writing of the paper.

Competing interests

The authors declare no competing interests.

Additional information

Supplementary information The online version contains supplementary material available at <https://doi.org/10.1038/s41467-025-64305-1>.

Correspondence and requests for materials should be addressed to Zhenzhong Zeng.

Peer review information *Nature Communications* thanks the anonymous reviewers for their contribution to the peer review of this work. A peer review file is available.

Reprints and permissions information is available at <http://www.nature.com/reprints>

Publisher's note Springer Nature remains neutral with regard to jurisdictional claims in published maps and institutional affiliations.

Open Access This article is licensed under a Creative Commons Attribution-NonCommercial-NoDerivatives 4.0 International License, which permits any non-commercial use, sharing, distribution and reproduction in any medium or format, as long as you give appropriate credit to the original author(s) and the source, provide a link to the Creative Commons licence, and indicate if you modified the licensed material. You do not have permission under this licence to share adapted material derived from this article or parts of it. The images or other third party material in this article are included in the article's Creative Commons licence, unless indicated otherwise in a credit line to the material. If material is not included in the article's Creative Commons licence and your intended use is not permitted by statutory regulation or exceeds the permitted use, you will need to obtain permission directly from the copyright holder. To view a copy of this licence, visit <http://creativecommons.org/licenses/by-nc-nd/4.0/>.

© The Author(s) 2025

Acknowledgements

This study was supported by the National Natural Science Foundation of China (42371026, 42071022), Shenzhen Science and